

Dynamic and Static Properties of Double-Layered Compound Acoustic Black Hole Structures

Tong Zhou^{*}, Liling Tang^{*}, Hongli Ji^{*†}, Jinhao Qiu[†] and Li Cheng^{*‡}

^{*}Department of Mechanical Engineering

The Hong Kong Polytechnic University, Hung Hom

Kowloon, Hong Kong SAR, P. R. China.

[†]State Key Laboratory of Mechanics and Control of Mechanical Structures

Nanjing University of Aeronautics and Astronautics, Nanjing 210016, P. R. China

[‡]li.cheng@polyu.edu.hk

The ‘Acoustic Black Hole’ (ABH) phenomenon shows it promises (or promising) in suppressing flexural vibrations in beam and plate structures. Conventional ABH structures, however, are tied with the inherent structural weakness due to the low local stiffness required and possibly high stress concentration caused by the small residual cross-section thickness of the ABH taper, thus hampering their practical applications. In this study, the dynamic and static properties of a compound ABH beam are investigated through numerical simulations. It is shown that, whilst ensuring effective ABH effect, the compound ABH structure allows a significant improvement in the static properties of the structure. For the former, the compound design is shown to outperform its counterpart in the conventional ABH configuration in terms of damping enhancement and vibration suppression. For the latter, the compound ABH structure is also shown to provide much better static properties in terms of structural stiffness and strength. Meanwhile, the structural damping can be further improved by using an extended platform at the tip of power-law profile, which meanwhile improves the structural strength but reduces the structural stiffness. Therefore, when choosing the platform length, a balance needs to be struck among the desired ABH effect and the mechanical properties of the structure.

Keywords: Acoustic Black Hole; vibration control; damping; static analysis; compound ABH structure.

1. Introduction

Suppressing flexural vibration in thin-walled structures like beams and plates is of great importance [Jones, 2001; Mead, 1998]. Surface coating with viscoelastic damping materials proves to be a popular way to increase system damping at the expenses of increasing the weight of the structure, be it for full or partial coverage. The former is most likely to be used for multi-resonance suppressions [Jones, 2001]. In recent years, there has been an increasing research interest in exploring the so-called ‘acoustic black hole’ effect for effective, lightweight and broadband vibration suppression purposes. It was shown that, through tailoring the structural thickness according to a power law profile (in the beam case for example, the beam thickness $h(x) = \varepsilon x^m$, $m \geq 2$), the local phase and group velocity of the bending wave gradually reduces, theoretically reaching zero in the tapered area when the thickness becomes zero [Mironov, 1988]. As a result, no energy will, in principle, be reflected at the wedge tip in the ideal case. The structural thickness, however, would never reach zero in reality due to the limited machining and manufacturing capability. This would result in a significant increase in the reflection coefficient, which can be countered, to certain extent, by the deposition of a thin damping layer only over the surface of the tapered wedge where the energy is focalized exhibiting large amplitude vibrations [Krylov, 2004; Krylov & Tilman, 2004; Krylov & Winward, 2007].

Various configurations with embedded ABH features have been proposed in the literature for enhancing the ABH effect on one hand, and for increasing the applicability of the structures on the other hand. By extending the tip of the power-law profiled wedge, a platform can be formed to prolong the area with large vibration amplitude, thus maintaining appreciable ABH effect even with a remaining structural thickness [Bayod, 2011]. Multi-layered ABH terminations with damping material applied between the layers have also been investigated through the measurement of the reflection coefficient and comparisons with a single layered wedge [Pelat *et al.*, 2015]. To avoid damages of the

fragile thin wedge tip and reduce the sharp tip for safety reason, attempt has been made to place the one-dimensional ABH tip into the inner part of a structure. Similarly, ABH feature has also been embedded and combined in various ways into plates, in the form of either quasi-one-dimensional power-law-profiled slots [Bowyer & Krylov, 2016; O'Boy & Krylov, 2016] or two-dimensional tapered circular indentations [O'Boy *et al.*, 2010; O'Boy *et al.*, 2011; Bowyer & Krylov, 2014]. As a different application, a beam with tapered centre ABH sections has also been investigated using a 2D FEM model for piezoelectric-based energy harvesting [Zhao *et al.*, 2014].

Conventional structures with embedded ABH features are tied with the inherent structural weakness because of the low local stiffness required and possibly high stress concentration caused by the small residual cross-section thickness of the ABH taper. This makes them difficult to be used for real-world applications, except for some cases where they are used as non-load-bearing components for which the requirement of mechanical rigidity is not a major concern [Bowyer & Krylov, 2014; Ji HL *et al.*, 2017]. Efforts were made to address this issue such as increasing the residual thickness of tailored profile [Unruh *et al.*, 2015], avoiding non-profiled centre holes [Feurtado & Conlon, 2016], embedding additional plateau [Huang *et al.*, 2016] for the tapers, reducing the number of indentations [Unruh *et al.*, 2015] or tailoring ABH profile merely on one of two surfaces of a honeycomb sandwich panel [Bowyer & Krylov, 2014]. Whilst compromising the ABH effect, these measures, however, lead to marginal improvement in the structural stiffness, which is still not enough for practical applications.

As one of the possible design configurations, a double-layered compound ABH configuration was proposed and briefly discussed in a previous work [Bowyer & Krylov, 2014]. Frequency response at the excitation point of a plate with high intrinsic loss factor containing compound ABH was measured experimentally and compared with the traditional simple ABH design. Intuitively, the double-layered compound ABH design could possibly improve the structural properties (in terms of both overall stiffness and stress concentration). The issue, however, has not been systematically assessed and quantified.

In this paper, a systematic assessment and investigations on the dynamic and static performance of a one-dimensional double-layered compound ABH structure are carried out using finite element analyses. The double layered ABH feature is embedded in the hosting beam-like structure, with integrate and smooth surface like a uniform beam. Previous one: Dynamic-wise, the vibration characteristics of such structures are first investigated using metrics defined in previous work [Tang *et al.*, 2016; Tang & Cheng, 2016, 2017], with comparisons with conventional ABH beams. Dynamic-wise, the vibration characteristics of such structures are first investigated with comparisons with conventional ABH beams by metrics used in previous work based on wavelet decomposition [Tang *et al.*, 2016; Tang & Cheng, 2016, 2017], which is also used for shape optimization of acoustic enclosure [Zhang & Cheng, 2015]. Both modal and structural damping analyses are performed, followed by energy distribution analyses under a point force excitation. Tapered beams with different profile parameters are investigated. Static-wise, the overall stiffness and strength of the ABH tapered structure are assessed. An additional platform is embedded into the compound ABH beam for further damping enhancement. Static analyses are also conducted on such modified double-layer structures to investigate the influence of the platform length. Experimental measurement was also conducted to confirm the validity of the FEM analyses as well as the superior ABH effect of the compound ABH beams.

2. Double-layered Compound Structure and FEM Model

Beams with two types of embedded ABH profiles are investigated, as shown in Fig.1. The conventional simple ABH (Fig. 1 (a)) and the compound ABH (Fig. 1 (b)) beams are built from the same basic geometry (Fig. 1 (c)) through horizontal and vertical symmetry. The basic geometry is a beam with an ABH termination, which can be divided into two parts: an ABH portion from x_0 to x_1 , and a uniform portion. The ABH portion follows a power-law thickness profile, *i.e.* $h(x) = \varepsilon(x - x_0)$ and a platform (from to) at the tip of the ABH portion with a constant residual thickness . The basic geometry is just used for illustrations and not used in the following analysis. A damping layer of constant thickness is added on both outer surfaces of ABH portion

for damping enhancement. For practical application of compound ABH, the damping layers could also be attached on the inner surfaces without altering damping effect evidently.

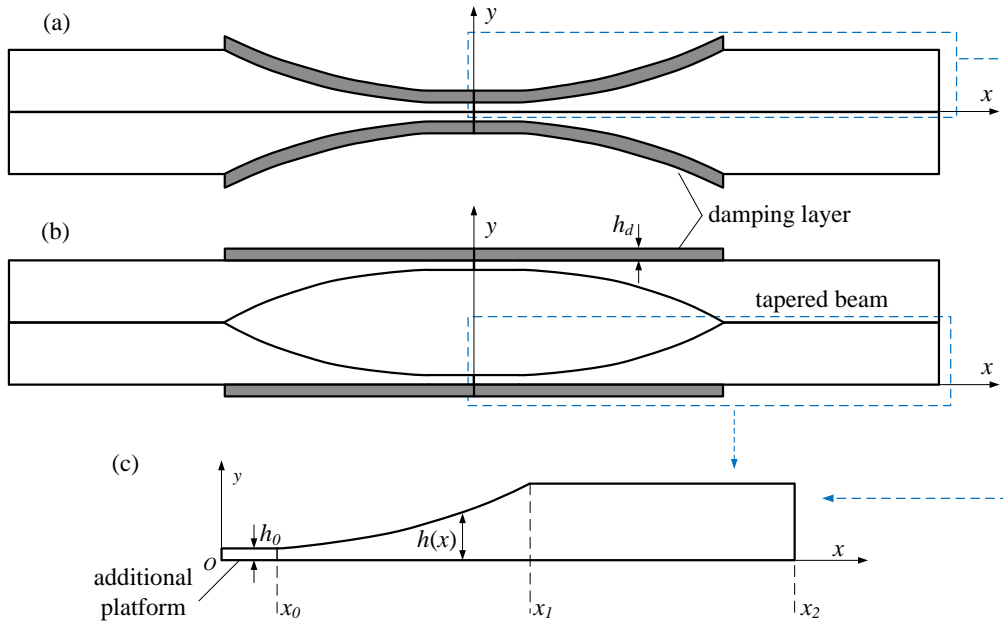


Fig. 1. Structure configurations with ABH profiles: (a) Conventional simple ABH, (b) double layered compound ABH, (c) basic geometry

Finite element simulations using COMSOLTM [Comsol, 2007] were used for both dynamic and static analyses. A 2D tapered beam model was developed under the plane stress conditions in solid mechanics interface. The left and right ends of the beams were set to be clamped and free, respectively. The damping layer, of constant thickness was assumed to be perfectly bonded with the tapered region of the beam and applied on the outside surface over the ABH portion for both the compound and simple ABH beams. Geometrical and material parameters, assigned to different parts of the beam, are tabulated in Table 1. The beam was meshed with triangular elements and the damping layers were meshed with quadrilateral elements. For dynamic analyses, the resolution of the mesh was chosen to be fine enough to reveal the details of vibration in the tapered area and the mesh size was set to ensure more than ten elements per wavelength at the highest frequency of interest. For static analyses, a convergence study was performed to ensure the accuracy and reliability of the results [Tabatabaian, 2016]. The number and resolution of mesh in tapered region were increased by setting the controlling parameter: resolution of narrow regions. The appropriate nonlinear solvers were also employed for eliminating the calculation errors during the simulation process for some specific cases.

Table 1. Parameters used in the simulations

Geometrical parameters	Material parameters
$\varepsilon = 0.005 \text{ cm}^{-1}$	Beam
$m=2$	$E_b=210 \text{ GPa}$
$h_b=0.125 \text{ cm}$	$\rho_b=7800 \text{ kg/m}^3$
$h_d=0.01 \text{ cm}$	$\eta_b=0.005$
	Damping layer
$x_0=0 \text{ cm}$	$E_d=5 \text{ GPa}$
$x_1=5 \text{ cm}$	$\rho_d=950 \text{ kg/m}^3$
$x_2=10 \text{ cm}$	$\eta_d=0.3$

Two indices, an equivalent compliance factor and a stress concentration factor, are defined to evaluate the static performance of ABH-featured beams, respectively. The so-called Equivalent Compliance Factor (ECF) is defined as the ratio between the maximum displacement of the beam with ABH and that without ABH when a unit force is applied at the free end of the beam. Similarly, with a unit moment applied at the free end, the ratio of the maximum stress between the beam with ABH and the one without ABH is defined as the Stress Concentration Factor (SCF) [Hibbeler, 2011]. The lower ECF is, the better the static performance of ABH beam is, and same applies to SCF. The influence of the damping layer was neglected when conducting the static analysis, due to its weak stiffness as compared to that of the host structure.

3. Simulation Results and Discussions

3.1. Dynamic and static analyses and comparison Studies

In this section, the vibration characteristics of the compound ABH beam are investigated and compared with the conventional simple ABH without additional platform.

Three compound ABH beam cases, labelled as C1, C2 and C3, are investigated and compared with their three conventional simple ABH counterparts, labelled as S1, S2 and S3. Through changing the residual thickness of the basic geometry $h_0 = h(x_0)$, all cases with different cross-section thickness can be built, as shown in Table 2. The cross-sectional thickness of the tapered ABH structure increases from Case C1 to C3 and from Case S1 to S3, respectively. Note the thickness is the same for all the study cases with the same case number.

Table 2 truncation thickness of compound ABH and Simple ABH of study cases

Compound	Simple	h_0
Case C1	Case S1	0.005 cm
Case C2	Case S2	0.01 cm
Case C3	Case S3	0.015 cm

Modal analyses are first conducted to reveal the vibrational characteristics of the compound ABH structure. Fig. 2(a) shows the system loss factors of all the flexural modes of the compound ABH structure, which can be divided into two groups: in-phase modes and out-of-phase modes. For the former, the displacements of the upper and bottom branches at any given cross-section are the same. For the latter, they have the same amplitude in the ABH region but in opposite directions, with no vibration energy distributed in the uniform beam region (upon omission of the Poisson's effect), as shown in Fig. 2(b). For the same residual thickness, the out-of-phase modes are shown to have larger system loss factors than that of the in-phase modes (Fig. 2(a)) because of their larger curvatures at the junction area between the uniform portion and ABH portion of the beam. This induces larger bending energy stored and dissipated by the damping layers. Meanwhile, all the energy of the out-of-phase modes is concentrated in the ABH portion where damping layer is applied. Note if the excitation is applied over the uniform part of the structure, the out-of-phase modes cannot be activated. The out-of-phase modes are treated as the local modes and therefore the following numerical analyses will only focus on the in-phase modes for the sake of simplicity. Fig. 2(a) also shows that, for the same group, compound or simple one, a thinner residual thickness will result in better system damping increase, in agreement with results reported in the literature for simple ABH structures.

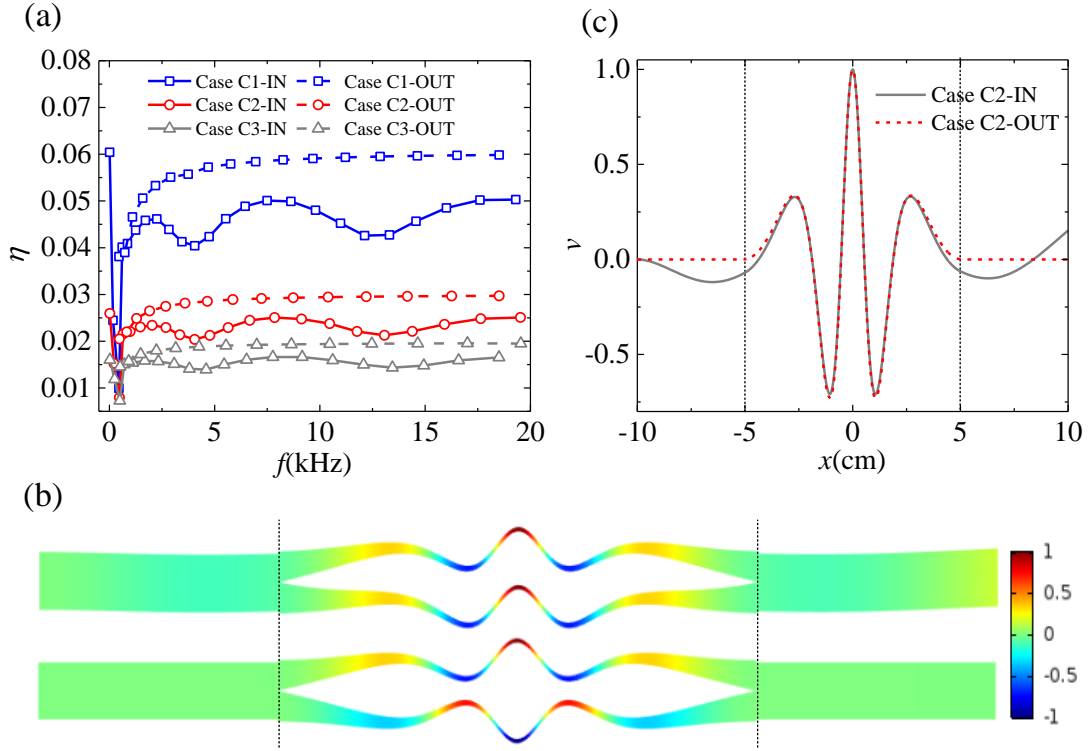


Fig. 2. (a) Comparison of system loss factors of the compound ABH structures between in-phase modes and out-of-phase modes (b) and (c) The 8th in-phase mode shape of compound ABH with the corresponding out-of-phase mode shape (normalized displacement)

Figure 3(a) compares the system loss factors of the compound and simple ABH tapered structures with different cross-sectional thickness. A uniform reference beam with the same length and height (uniform part) as case C2 or S2 is also considered for comparison purposes. The loss factor assigned to the material of the beam is 0.005. The ABH region does not dominate the vibration mode at the first three structural modes (below 500 Hz). For higher resonant frequencies, the system loss factors are systematically increased owing to the ABH effect, much more appreciable with a thinner residual thickness for both compound and simple ABH beams. Comparisons between the two types of beams, however, reveals higher system loss factors for the compound ABH beams, as compared with the conventional simple ones, with the same cross-sectional thickness and total structural weight. This indicates that the compound ABH structures not only exhibit the expected ABH effect for system damping enhancement, but also outperform the conventional simple ABH structures. Figure 3(b) shows more details of the system loss factors within the frequency band between 500 Hz and 7000 Hz. It can be seen that the compound beam seems to exhibit ABH effect at a lower frequency (squares in Fig. 3(b)) as compared to the conventional simple one. The resonance frequencies of the 8th mode of Case S2 and Case C2 are 4044 Hz and 2688 Hz, respectively (black circles in Fig. 3(b)). Meanwhile, the compound ABH structure also seems to have a higher modal density than the simple one.

To further examine the details, the 8th in-phase mode shape of the compound ABH is depicted as a representative example and compared with its counterpart of the simple ABH beam in Fig. 3(c). It can be seen that the wavelength becomes shorter in the ABH region for both the compound and simple ABH beams, testifying the typical ABH phenomenon in terms of the reduction of the local phase velocity of flexural waves. Compared with simple ABH, however, the compound ABH structure undergoes a larger deformation in the ABH region ($-5 < x < 5$), thus resulting in higher modal loss factors, as demonstrated before. Results of the normal strain distribution (Fig. 3(d)) show that a neutral axis appears in both upper and bottom branches of the compound ABH beam for all in-phase modes, suggesting that each branch of the compound ABH beam bends individually under dynamic excitation. Since the thickness of one branch of the compound ABH beam is only half of the simple one at same cross section location, one individual tapered branch of the compound beam has a lower local dynamic

stiffness than the simple ABH taper. Therefore, this not only accelerates the wave speed reduction, but also leads to larger local deformation and higher energy concentration in the tapered area. Moreover, the lower dynamic stiffness of each compound ABH arm also results in a lower cut-on frequency and a higher modal density.

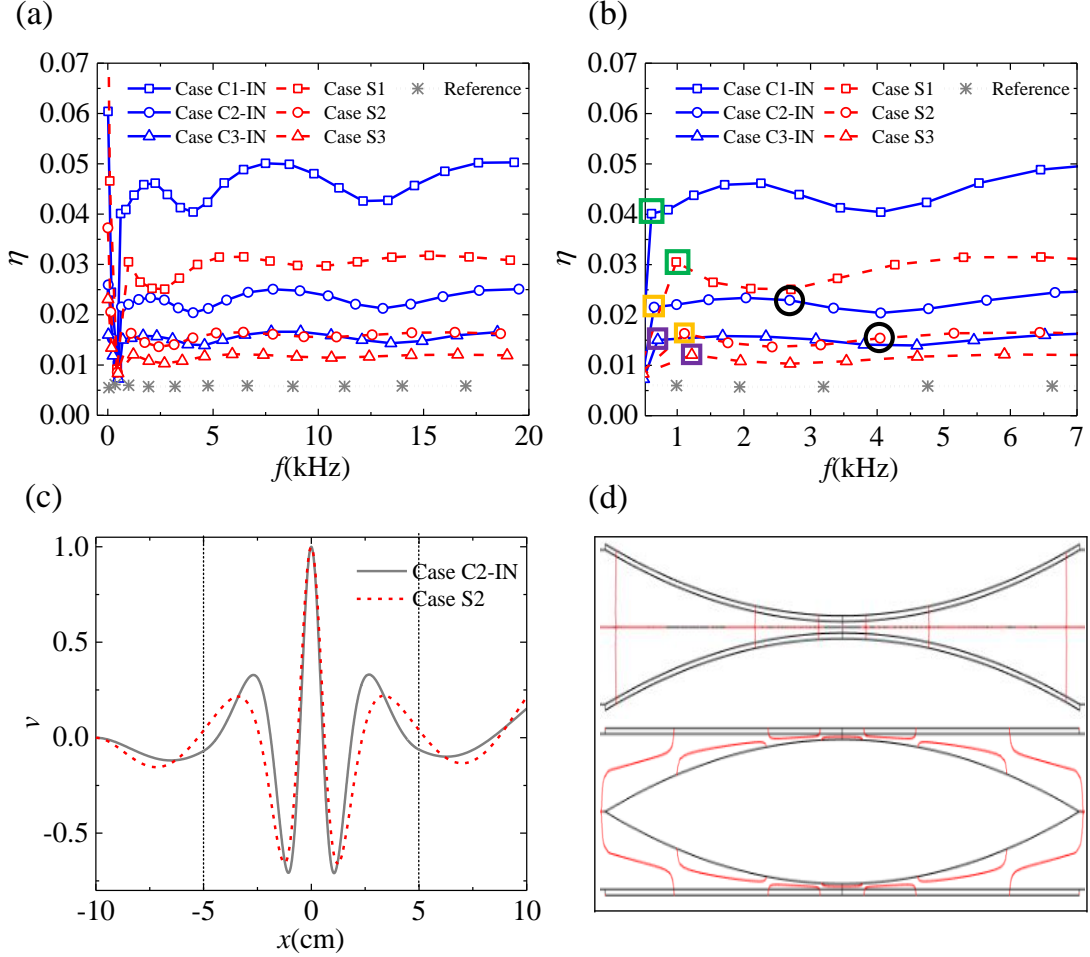


Fig. 3. (a) system loss factors of compound and simple ABH beams. (b) system loss factors of compound and simple ABH beams within a narrow frequency band (c) 8th in-phase mode shape of compound and simple ABH beams (normalized displacement) (d) the 0-value contour line of strain in x direction within the ABH portions of the 8th mode of simple and compound ABH beams (without deformation and not the realistic aspect ratio used in simulation).

To further show and demonstrate the ABH effect of the compound structure, the vibration level of the structures is analyzed using their quadratic velocity, averaged over the uniform portion. Meanwhile, to better characterize the energy transfer phenomenon, an energy ratio term, Γ , is defined as $\Gamma = 10 \log (\langle V^2 \rangle_{\text{ABH}} / \langle V^2 \rangle_{\text{Unif}})$, in which the two terms involved are the mean quadratic velocity of ABH part and that of the uniform part, respectively, under forced vibration. A point force excitation of unit amplitude was applied at 3 cm away from free end of beam in the y axis direction. As a comparison basis, the uniform beam is also calculated by taking the same beam elements corresponding to the ABH beam. Results are shown in Figs. 4 (a) and (b). It can be seen from Fig.4(a) that the vibration level of the uniform part of both ABH tapered structures is generally lower than that of the reference beam when frequencies increase, evidenced by the positive Γ for most frequencies. Compared with the simple ABH design, the peaks of mean quadratic velocity of the uniform part of the compound ABH are lower, which is consistent with the result of the calculated system loss factors. Meanwhile, compound ABH shows higher energy focalization over most frequency band than simple ABH and the energy ratio Γ of both ABH tapered structures is much higher than reference beam. The

dip in the energy ratio Γ curves around 10 kHz is the phenomenon of loss of ABH effect observed in a finite beam structure [Tang & Cheng, 2016].

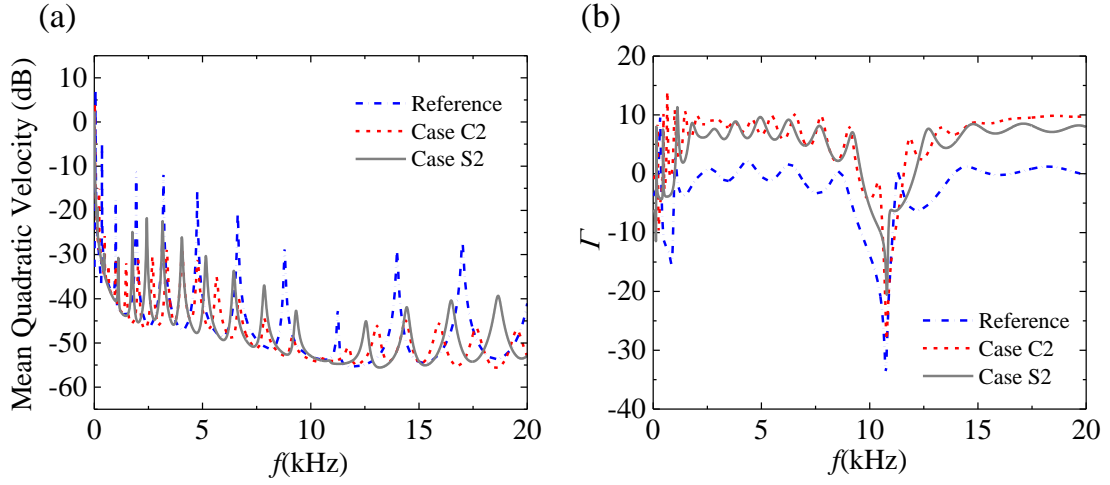


Fig. 4. (a) Mean quadratic velocity of uniform portion and (b) ratio of mean quadratic velocity of the ABH portion to uniform portion

Static analyses are conducted to compare static properties of compound ABH with traditional simple ABH design. The calculated Equivalent Compliance Factor (ECF) and the Stress Concentration Factor (SCF) are tabulated in Table 3. It can be seen that both the static deformation and the stress of the compound ABH under external static loading are much lower than their counter parts in the traditional simple ABH. With the increase of the cross-sectional thickness, the static performance of both structures is improved at the expenses of compromising the ABH effect.

Table 3 Static study of compound ABH and Simple ABH structure

Equivalent compliance factor (ECF)			
Case S1	769.2	Case C1	12.43
Case S2	156.3	Case C2	5.66
Case S3	63.7	Case C3	3.83
Stress concentration factor (SCF)			
Case S1	674	Case C1	16.96
Case S2	182	Case C2	8.63
Case S3	87.1	Case C3	5.87

To further confirm the advantages of the compound ABH beam over simple one, the parameters of the power-law profile ($h(x) = \varepsilon(x - x_0)^m + h_0$) in Table 1 are varied in the following analyses. The reduction of the length of ABH portion in the basic geometry is around 2 cm when ε is changed to 0.014 or m is increased to 3, respectively. When the wavelength of the free bending wave equals to the length of ABH portion, ABH begins to act as a broadband absorber and the corresponding frequency of the flexural wave is defined as the cut-on frequency [Feurtado & Conlon, 2016]. The highest cut-on frequency of the studied cases is approximately 6500Hz. Since no significant fluctuation of the loss factor is noticed at higher frequencies, a frequency band above the cut-on frequency is chosen for the calculation of average system loss factor, which ranges between 7 kHz and 20 kHz in the present case.

Figure 5 presents the effect of residual thickness on the increase of average loss factor of compound ABH compared with simple ABH for different profile parameters ($\Delta\bar{\eta} = \bar{\eta}_{compound_ABH} - \bar{\eta}_{simple_ABH}$). It can be seen that compound ABH has better overall ABH effect in terms of damping than the simple

ABH beam, evidenced by $\Delta\bar{\eta}$, all larger than 0. With the increase of the residual thickness h_0 , this difference is narrowed as $\Delta\bar{\eta}$ decreases. Meanwhile, a larger m results in higher increase of the average loss factor compared with simple ABH while the increase of the parameter ε shows adverse effect on $\Delta\bar{\eta}$. All in all, the above analysis shows that the compound design shows its overwhelming advantage over the conventional simple one when the structure becomes structurally venerable (rapid thickness changes and thinner residual truncated thickness).

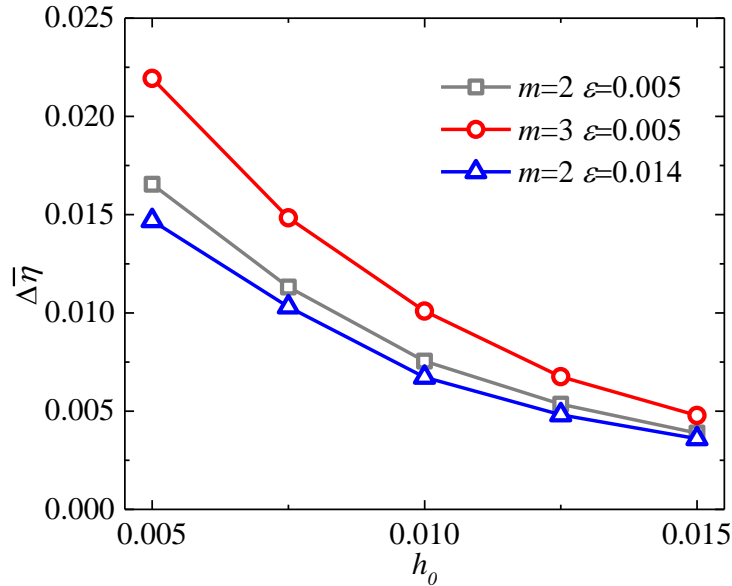


Fig. 5. Increase of average loss factor of compound ABH compared with simple ABH

Corresponding changes in the static properties are then investigated using two parameters, R_E and R_S , defined as the ratios of ECF and SCF between compound ABH and simple ABH, respectively. As shown in Fig. 6, both R_E and R_S become larger with the increase of residual thickness and both ratios are lower than 0.1 for every set of the profile parameters and the selected residual thickness, suggesting that the compound ABH outperforms the single ABH beam. With the increase of the residual thickness h_0 , the static performance difference between the compound and simple ABH beam becomes smaller. The points of R_S overlap for the same taper power with different ε .

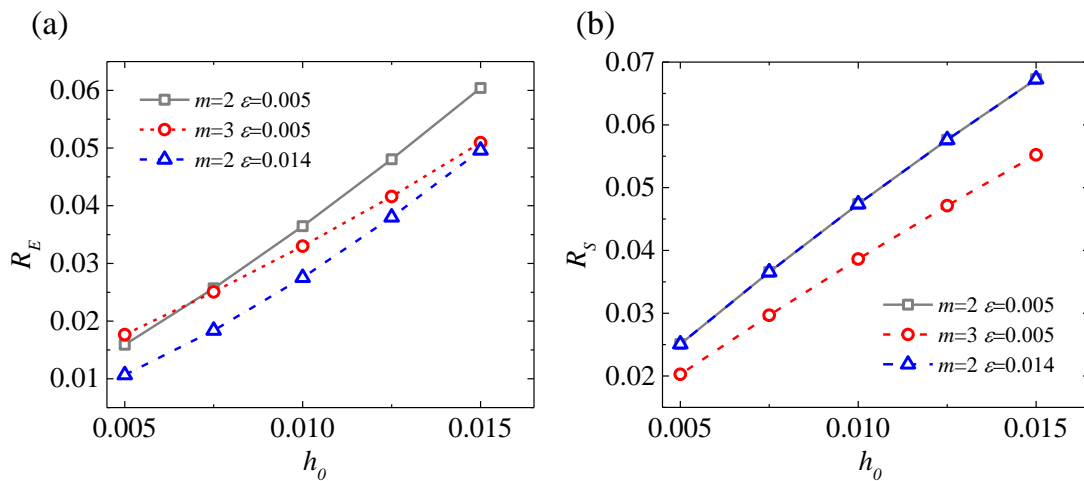


Fig. 6. (a) Equivalent compliance factor ratio of compound ABH and simple ABH (b) stress concentration factor ratio of compound ABH and simple ABH

3.2. Improvement of the compound ABH effect with additional platform

The truncated tip in the basic geometry (Fig. 3(c)) can be extended with a constant thickness to form a platform to enhance traditional 1D ABH effect [Bayod, 2011; Tang & Cheng, 2017]. An additional platform is added to the basic geometry of the compound ABH structure. The length of the platform in the basic geometry is defined as $p = |0 - x_0|$, leading to a total length $2p$. The additional platform is also treated as the ABH portion, covered by a damping layer with constant thickness h_d .

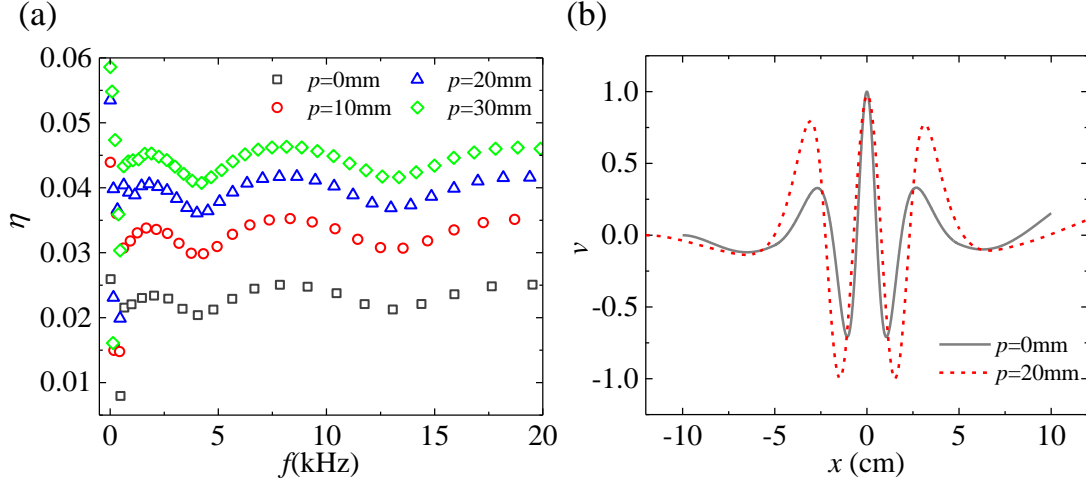


Fig. 7. (a) System loss factors of Case C2 with different lengths of addition platform (b) 8th in-phase mode shapes of Case C2 with and without addition platform (normalized displacement)

Numerical analyses are performed to reveal the influence of the platform on compound ABH effect using the geometric parameters in Case C2. Figure 7(a) shows that a longer platform in the compound ABH generates larger system loss factors and higher modal density after the first few structural modes. Meanwhile, the introduction of the platform reduces the cut-on frequency due to the increase in the length of ABH region, thus lowering down the effective region of the ABH effect. The tendency in the loss factor is complex for the first few resonant frequencies but becomes systematic in the higher frequency range for different platform lengths. To further explain the increase in the loss factors due to the platform, the mode shape of an arbitrarily chosen mode (8th in the present case) with and without platform are depicted and compared in Fig. 7(b). It can be seen that the additional platform results in more severe flexural vibrations of the ABH region as well as the deformation of the damping layer, both promoting better ABH effect. With the platform, the length of the ABH region is increased from 10cm to 14cm and the area with larger flexural displacement is also spread out because of the extension of the residual thickness.

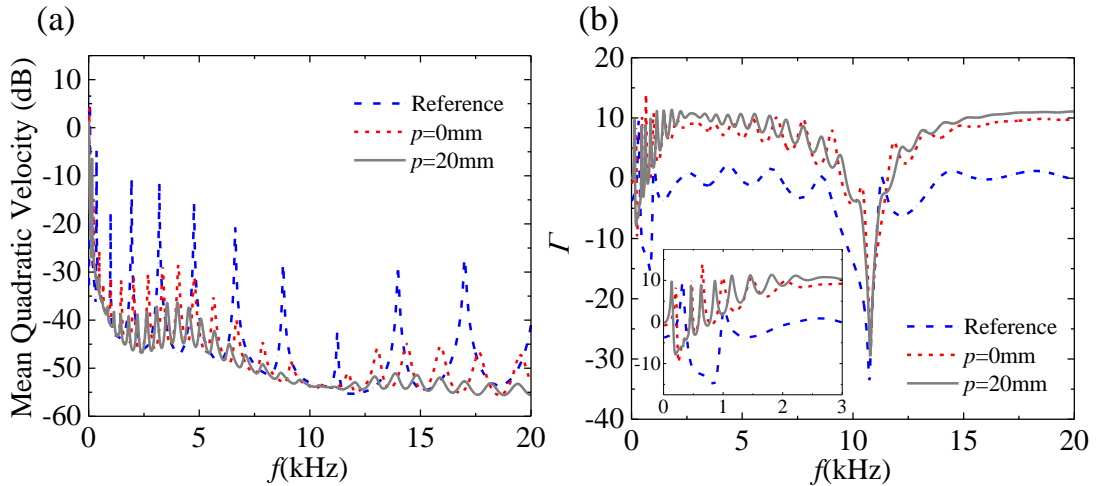


Fig. 8. Mean quadratic velocity of uniform portion and ratio of mean quadratic velocity of the ABH portion to uniform portion of Case C2 with addition platform.

Figure 8 illustrates the averaged mean quadratic velocity of uniform portion and the energy ratio Γ , with and without platform for the compound ABH beam. The reference is a uniform beam with the same length and thickness (uniform portion) as Case C2. Changes in the major peaks in the mean quadratic velocity curves of the uniform portion show the damping effect of the ABH. Compared with the original Case C2, the vibration level in the uniform region is further reduced by the ABH beam with platform and such a reduction is more obvious after 12.5 kHz. As shown in Fig. 8 (b), more vibration energy is shifted to the ABH portion and more peaks appear in the curves of energy ratio due to the energy concentration effect provided by additional platform, in comparison with the ABH beam without platform. When the profile parameters are changed, the platform can also improve the average system loss factor of compound ABH, as shown in Fig. 9. Higher taper power index leads to better damping effect for a given platform length. Compared with the original profile, the average loss factors with a larger profile parameter ε is lower for shorter platform and becomes larger for longer platform. Better ABH effect for damping flexural vibration can be achieved through longer platform but the increasing tendency of $\bar{\eta}$ slows down for larger p .

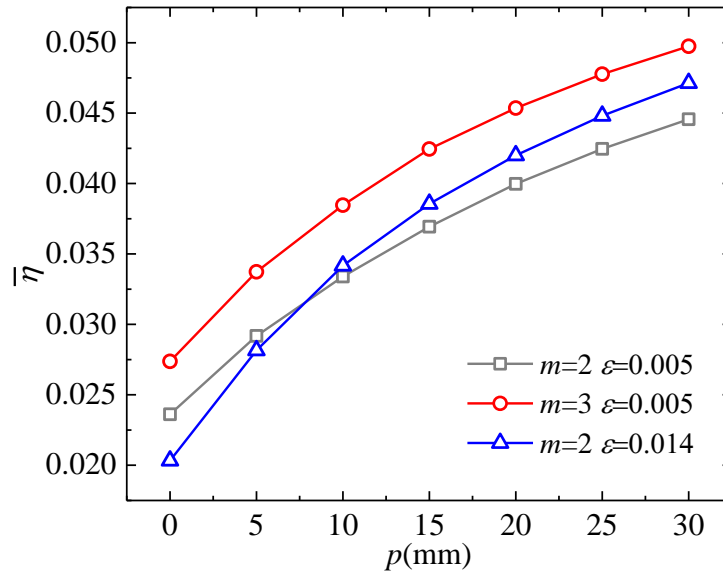


Fig. 9. Average loss factor of compound ABH with different length of platform

Embedding additional platform into the compound ABH can also change the static properties of the tapered structure. With the increase of the platform length, Fig. 10(a) shows the ECF becomes larger since the additional platform reduces the stiffness of the beam as compared with the reference beam, which has the same thickness (uniform portion) and length with ABH tapered structure. However, it can be seen from Fig. 10(b) that the SCF decreases within a certain range of the platform length, suggesting that the additional platform can improve the strength of compound ABH structure within a certain range, after which the stress concentration factor increases and the position of maximum stress changed from the centre of the platform to the connection point between the platform and taper wedge with a lower power profile. This trade-off needs to be taken into account when designing a compound ABH structure with additional platform. In addition to the damping effect enhancement, the strength and stiffness of compound ABH structure with additional platform needs to be balanced, as shown in Fig. 10(c).

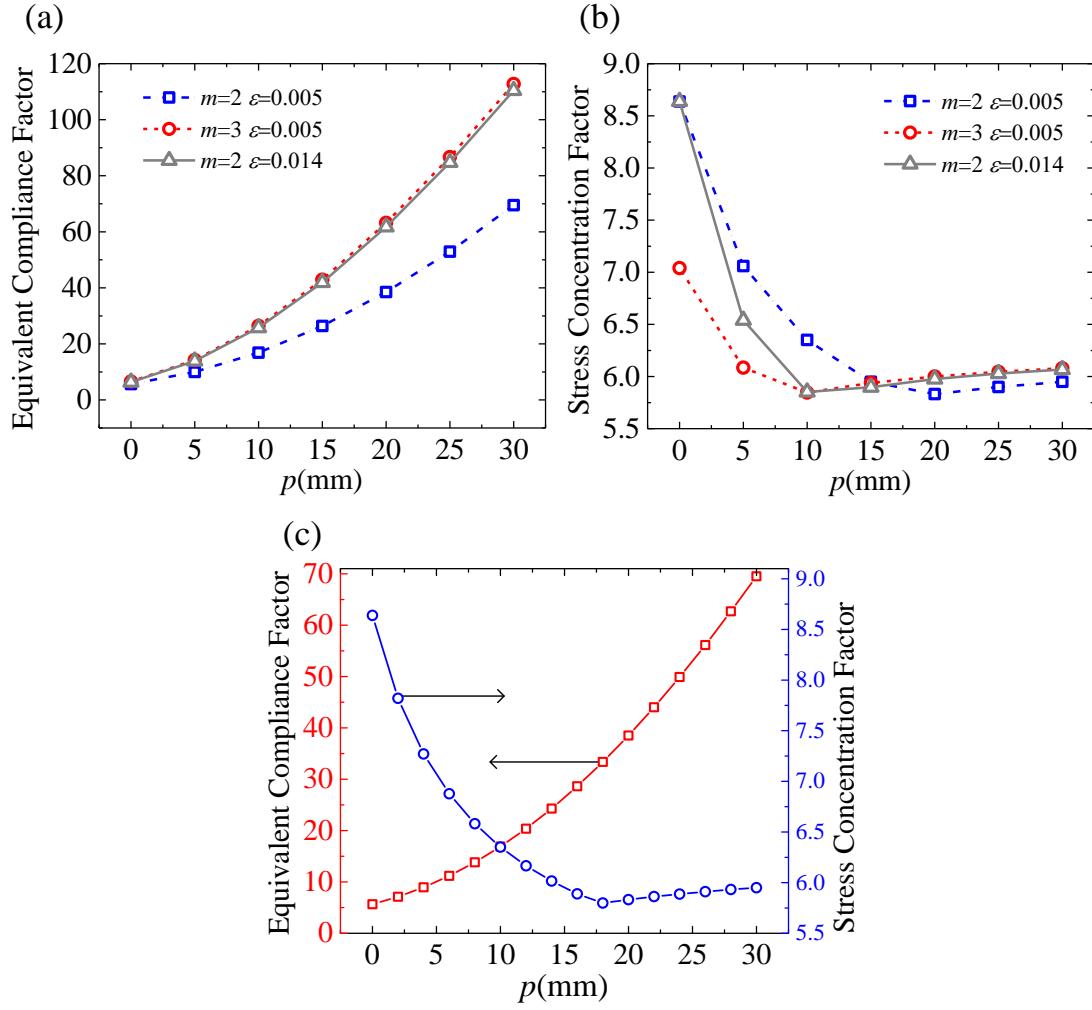


Fig. 10. (a) Equivalent compliance factor of the compound ABH with different platform lengths (b) Stress concentration factor of the compound ABH with different lengths of platform (c) Static study of Case C2 ($m=2, \varepsilon=0.005$) with different platform lengths

4. Experimental Validation of Dynamic Analysis

Experiments were conducted to verify the predicted ABH effect of the compound ABH beam, as well as the reliability of the numerical analyses.

A double-layered hollow tapered beam was manufactured by electro discharge machining (EDM), which can produce complex geometry parts and process hard-to-machine materials. The material of the tapered beam was chosen to be steel to ensure sufficient structural residual strength during manufacturing and enough mechanical rigidity under external disturbance. The starting location of the machining process was chosen to be the cross section connecting the uniform portion and ABH portion to avoid large plastic deformation. For numerical simulations, the mass density and Young's modulus of the beam were 7741 kg/m^3 and 200 GPa , respectively. The inherent loss factor was estimated to be 0.001 , which is within the nominal range provided in the literatures [Berger & American Industrial Hygiene, 2000; Mead, 1998]. Other ABH parameters were: $m=2$, $\varepsilon=0.014 \text{ cm}^{-1}$, $h_0=0.05 \text{ cm}$, $h_b=0.35 \text{ cm}$, $x_0=0 \text{ cm}$, $x_1=5 \text{ cm}$, $x_2=15.5 \text{ cm}$. The width of whole beam was 1.9 cm .

The attached damping film was an acrylic polymer 3MTM very high bond (VHB) adhesive transfer tape F9473PC. The same damping material was also used for estimating the loss factors of constrained layer damping treatment in Ref. [Liu & Ewing, 2007]. The density and Poisson's ratio of damping layers were 980 kg/m^3 and 0.499 , respectively. The related simulation model adopted constant values of shear modulus 10 MPa and loss factor 0.9 , corresponding to the frequency-dependent properties [Liu & Ewing, 2007] evaluated at 4000 Hz . The Young's modulus of the polymers was obtained from its

relationship with Poisson's ratio and shear modulus [Jones, 2001]. Only pressure was required to ensure adequate bonding of the damping tape at room temperature (21°C) according the technical manual provide by the manufacturer. A damping layer were built up by piling up many layers of thin adhesive tapes and such multi-layered treatment was also utilized in Ref. [Jones, 2001] for measuring the modulus and damping properties of the thin adhesive tapes. The combined damping layer had a final dimensions of $6 \times 1.9 \times 0.26$ cm, applied over the outside surface of the ABH portion, as shown in Fig. 11.

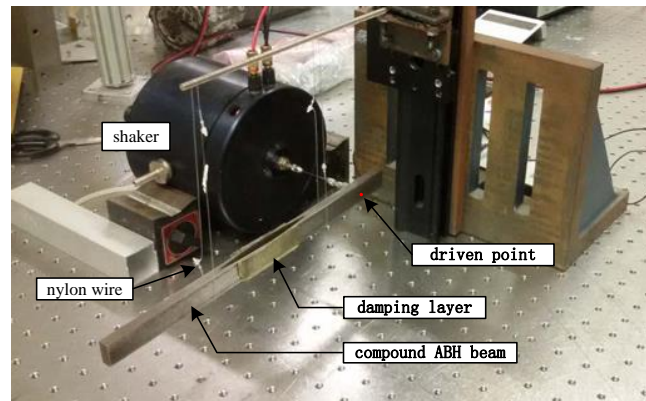


Fig. 11. Experimental set-up.

In order to achieve the free boundary conditions (to avoid the difficulty in realizing perfectly clamped edges), the compound ABH beam was suspended by two nylon wires from an independent frame, taking weight off the uniform portion of the tapered beam and introducing minimal damping to the system. An electromagnetic shaker, feed by a power amplifier (B&K 2706), was utilized to generate a periodic chirp signal (10-12000 Hz) at 3 cm away from the free end of the tapered beam. A flexible and slim stinger was used to connect the shaker with the beam through a force transducer (B&K 8203), providing the measured force signal to a charge amplifier (B&K 2635). The dynamic responses were measured by a PolytecTM laser scanning vibrometer (PSV 400).

The structural mobility at the driving point with and without damping layers is compared with FEM results in Fig. 12. Generally speaking, one notices a good agreement between the measured and simulated response curves. The ABH effect becomes obvious and dominant after 2000 Hz for the test compound ABH beam. The compound ABH beam becomes heavily damped with the deployment of the damping layers. For the undamped tapered beam (Fig. 12(a)), the estimated errors of natural frequencies of bending modes are less than 3%. Some fluctuations in the experimental response curve are likely caused by the torsional modes of slightly damped ABH beam and deviation of the excited force from the central axis, which is revealed by the overall structural responses (not shown here). As can be seen from Fig. 12(b), the measured curve is smoothed with the introduction of damping layer. The predicted damped response agrees well with experimental one.

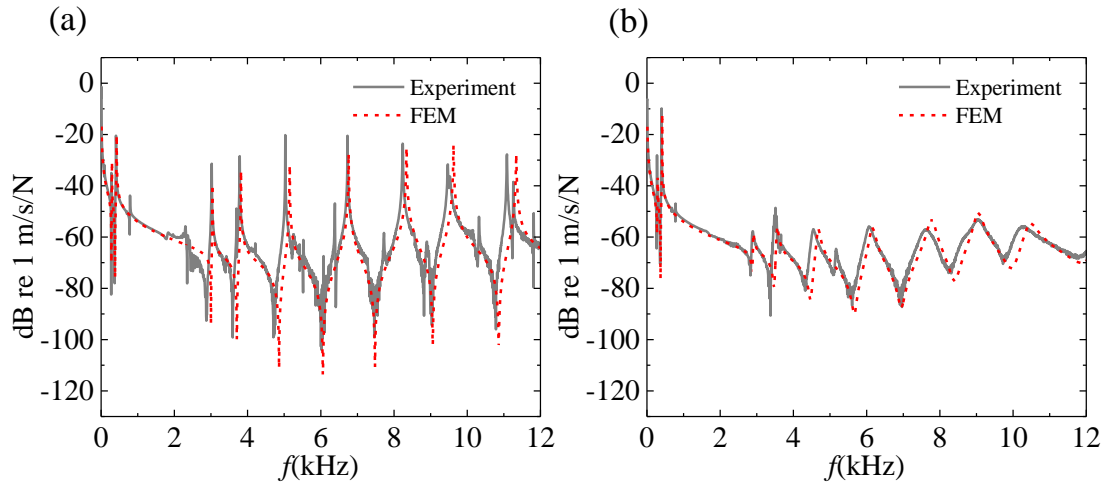


Fig. 12. Comparison between the measured and predicted driving point mobility of the compound ABH beam (a) without damping layers and (b) with damping layers.

5. Conclusions

In this study, a compound ABH beam is investigated from both dynamic and static perspective. Through modal analysis and forced vibration study, the compound ABH has been shown to produce significant ABH phenomenon, outperforming the traditional simple ABH design with same cross-section thickness and total structural weight in terms of structural damping enhancement and vibration suppressions, confirmed by experiments. Meanwhile, static analyses reveal that embedding compound ABH feature into beam can also offer much better mechanical strength and stiffness, for different profile parameters. Using an extended platform in the compound ABH can further improve the damping effect, similar as the case of traditional simple ABH wedges. However, a trade-off needs to be taken into consideration when choosing the platform length. An increase in the platform length within a certain range increases the strength, but decreases its stiffness at the same time. Therefore, a balance needs to be struck among the desired ABH effect and the mechanical properties of the structure.

To sum up, as compared with conventional ABH beam design, the compound ABH structure is shown to produce effective ABH effect while ensuring better structural rigidity at the same time, which points to more feasible and practical applications in vibration control, noise reduction and energy harvesting applications.

Acknowledgments

The authors would like to acknowledge the Research Grant Council of the Hong Kong SAR (PolyU 152009/15E and PolyU 152026/14E) National Science Foundation of China (No. 11532006) and the NUA State Key Laboratory Program under Grant MCMS-0514K02 for financial support. They are also grateful to Chikyan Koo, from Industrial Centre of the Hong Kong Polytechnic University, for the manufacture of the compound ABH beams.

References

- Bayod, J. J. [2011] "Experimental Study of Vibration Damping in a Modified Elastic Wedge of Power-Law Profile," *Journal of Vibration and Acoustics*, 133(6), 061003.
- Berger, E. H.(ed.) [2003] *The noise manual (5th ed.)* (American Industrial Hygiene Association, Fairfax, VA).
- Bowyer, E. P. & Krylov, V. V. [2014] "Experimental investigation of damping flexural vibrations in glass fibre composite plates containing one- and two-dimensional acoustic black holes," *Composite Structures*, 107, 406-415.

- Bowyer, E. P., & Krylov, V. V. [2016] "Slots of power-law profile as acoustic black holes for flexural waves in metallic and composite plates," *Structures*, 6, 48-58.
- Comsol, A.B. [2007] *Comsol Multiphysics Reference Manual*.
- Feurtado, P. A. & Conlon, S. C. [2016] "An Experimental Investigation of Acoustic Black Hole Dynamics at Low, Mid, and High Frequencies," *Journal of Vibration and Acoustics*, 138(6), 061002.
- Hibbeler, R. C. [2011]. *Mechanics of materials (8th ed.)* (Prentice Hall).
- Huang, W., Ji, H., Qiu, J., & Cheng, L. [2016] "Wave Energy Focalization in a Plate With Imperfect Two-Dimensional Acoustic Black Hole Indentation," *Journal of Vibration and Acoustics*, 138(6), 061004.
- Ji HL, H. W., Qiu JH, Cheng L. [2017] "Mechanics problems in application of acoustic black hole structures[J],"(in Chinese) *Advances in Mechanics*, 47:201710.
- Jones, D. I. [2001] *Handbook of viscoelastic vibration damping* (John Wiley & Sons).
- Krylov, V. V. [2004] "New type of vibration dampers utilising the effect of acoustic'black holes'," *Acta Acustica united with Acustica*, 90(5), 830.
- Krylov, V. V., & Tilman, F. J. B. S. [2004] "Acoustic 'black holes' for flexural waves as effective vibration dampers," *Journal of Sound and Vibration*, 274(3), 605-619.
- Krylov, V. V., & Winward, R. E. T. B. [2007] "Experimental investigation of the acoustic black hole effect for flexural waves in tapered plates," *Journal of Sound and Vibration*, 300(1-2), 43-49.
- Liu, W., & Ewing, M. S. [2007] "Experimental and analytical estimation of loss factors by the power input method," *AIAA journal*, 45(2), 477-484.
- Mead, D. J. [1999] *Passive vibration control* (John Wiley & Sons Inc.).
- Mironov, M. A. [1988] "Propagation of a flexural wave in a plate whose thickness decreases smoothly to zero in a finite interval," (in English) *Soviet Physics Acoustics-Ussr*, 34(3), 318-319.
- O'Boy, D. J., Krylov, V. V., & Kralovic, V. [2010] "Damping of flexural vibrations in rectangular plates using the acoustic black hole effect," *Journal of Sound and Vibration*, 329(22), 4672-4688.
- O'Boy, D. J., D., Bowyer, E., & Krylov, V. [2011] "Point mobility of a cylindrical plate incorporating a tapered hole of power-law profile," *The Journal of the Acoustical Society of America*, 129(6), 3475.
- O'Boy, D., & Krylov, V. V. [2016] "Vibration of a rectangular plate with a central power-law profiled groove by the Rayleigh-Ritz method," *Applied Acoustics*, 104, 24-32.
- Pelat, A., Denis, V., & Gautier, F. [2015] "Experimental and theoretical study of the reflection coefficient of a ABH beam termination," *Proc. of the INTER-NOISE and NOISE-CON Congress and Conference*, Vol. 250, No. 2, pp. 5001-5009, Institute of Noise Control Engineering.
- Tabatabaian, M. [2016] *Comsol[®]5 for engineers* (Mercury Learning and Information, Dulles Virginia).
- Tang, L., Cheng, L., Ji, H., & Qiu, J. [2016] "Characterization of acoustic black hole effect using a one-dimensional fully-coupled and wavelet-decomposed semi-analytical model," *Journal of Sound and Vibration*, 374, 172-184.
- Tang, L., & Cheng, L. [2016] "Loss of acoustic black hole effect in a structure of finite size," *Applied Physics Letters*, 109(1), 014102.
- Tang, L., & Cheng, L. [2017] "Enhanced Acoustic Black Hole effect in beams with a modified thickness profile and extended platform," *Journal of Sound and Vibration*, 391, 116-126.

- Unruh, O., Blech, C. & Monner, H. P. [2015] "Numerical and Experimental Study of Sound Power Reduction Performance of Acoustic Black Holes in Rectangular Plates," *SAE International Journal of Passenger Cars-Mechanical Systems*, 8(2015-01-2270), 956-963.
- Zhang, S., & Cheng, L. [2015] "Shape optimization of acoustic enclosures based on a wavelet-Galerkin formulation," *International Journal of Applied Mechanics*, 7(01), 1550009.
- Zhao, L., Conlon, S. & Semperlotti, F. [2014] "Broadband energy harvesting using acoustic black hole structural tailoring," *Smart materials and structures*, 23(6), 065021.